

Moisture transport contributing to precipitation at the centre of storm Bronagh

Article

Published Version

Creative Commons: Attribution 4.0 (CC-BY)

Open Access

Cuckow, S., Dacre, H. F. ORCID: <https://orcid.org/0000-0003-4328-9126> and Martinez-Alvarado, O. ORCID: <https://orcid.org/0000-0002-5285-0379> (2022) Moisture transport contributing to precipitation at the centre of storm Bronagh. *Weather*, 77 (6). pp. 196-201. ISSN 0043-1656 doi: <https://doi.org/10.1002/wea.4212> Available at <https://centaur.reading.ac.uk/104763/>

It is advisable to refer to the publisher's version if you intend to cite from the work. See [Guidance on citing](#).

To link to this article DOI: <http://dx.doi.org/10.1002/wea.4212>

Publisher: Wiley

All outputs in CentAUR are protected by Intellectual Property Rights law, including copyright law. Copyright and IPR is retained by the creators or other copyright holders. Terms and conditions for use of this material are defined in the [End User Agreement](#).

www.reading.ac.uk/centaur

CentAUR

Central Archive at the University of Reading

Reading's research outputs online

Moisture transport contributing to precipitation at the centre of storm *Bronagh*

Weather – June 2022, Vol. 77, No. 6

Sophie Cuckow¹ , Helen F. Dacre¹  and Oscar Martínez-Alvarado² 

¹Department of Meteorology, University of Reading, Reading, UK

²National Centre for Atmospheric Science, University of Reading, Reading, UK

Introduction

The precipitation associated with extratropical cyclones can lead to flooding in the United Kingdom (UK). Furthermore, the intensity of cyclone precipitation and associated flooding is expected to increase in the future due to climate change (Allan and Soden, 2008). Therefore, it is important that we understand the mechanisms by which extratropical cyclones generate precipitation so that we can accurately forecast flood events and mitigate risk. Previous studies have shown that a cyclone-relative airflow, known as a warm conveyor belt (WCB), can generate precipitation extremes (Pfahl and Wernli, 2012), and additional research has found that features known as atmospheric rivers are associated with precipitation extremes in the UK (Lavers *et al.*, 2011, 2012).

Since the 1970s, the structure and evolution of cloud and precipitation features associated with extratropical cyclones have been described using the conveyor belt model. The conveyor belt model examines Eulerian wind fields on vertically sloping isentropic surfaces in a cyclone-relative framework (Browning and Harrold, 1970). In regions of weak horizontal temperature gradient, isentropic surfaces are approximately horizontal and potential temperature increases with height. However, in regions with sharp horizontal temperature gradients, isentropic surfaces slope in the vertical. Therefore, in the vicinity of fronts, poleward moving dry air parcels will ascend along sloping isentropic surfaces in order to conserve their potential temperature. Conversely, equatorward moving dry air parcels will descend along sloping isentropic surfaces in order to conserve their potential temperature. This results in 3-dimensional airflows associated

with fronts (Carlson, 1980). Poleward moving airflows transport moist air from the surface to the upper troposphere resulting in cloud and precipitation formation. Equatorward moving airflows transport dry air from the upper troposphere to the lower troposphere, resulting in cloud-free regions. However, isentropic flow alone does not explain the development of some cyclone cloud features which move rearwards relative to the motion of the moving cyclone. An example is the cloud head that emerges from beneath the frontal cloud band and wraps cyclonically around the cyclone centre as the cyclone develops. In order to explain what is seen in the satellite imagery, the moving cyclone must be taken as the frame of reference. By subtracting the cyclone motion vector from the wind vectors, the transition to a cyclone-relative framework is made and the cyclone-relative airflows, called conveyor belts, which form the conveyor belt model can be identified.

Figure 1 describes three cyclone-relative airflows in relation to the surface fronts, precipitation and moisture flux features (Dacre *et al.*, 2015). The poleward moving warm conveyor belt (red arrow labelled WCB in Figure 1) is a moist cyclone-relative airflow that ascends from the top of the boundary layer ahead of the cold front along a relatively warm isentropic surface, leading to cloud and precipitation formation (Browning, 1971). Typically, during the developing stages of cyclone evolution, the WCB ascends to the upper troposphere where it turns anticyclonically to form a cirrus shield. During the mature stage of cyclone evolution, a lower branch of the WCB can turn cyclonically to form the upper portion of the comma-shaped cloud head. The dry intrusion (yellow arrow labelled DI in Figure 1) is an equatorward moving cyclone-relative airflow that descends behind the cold front bringing dry air from the lower stratosphere and upper troposphere. It assumes a hammer-head shape behind the cold front as it descends and creates a cloud-free band between the cloud head and the cold frontal cloud band (Young *et al.*, 1987). The feeder air stream (green arrow labelled FA in Figure 1) is a moist cyclone airflow within the boundary layer of the cyclones

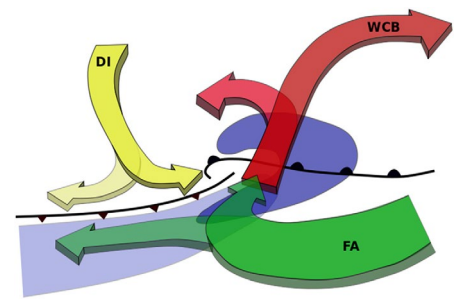


Figure 1. Cyclone-relative airflows within an extratropical cyclone. The warm conveyor belt (WCB, red), dry intrusion (DI, yellow) and feeder air stream (FA, green) are depicted by the coloured arrows. Also shown are the surface fronts (black), high integrated vapour transport (light blue shading) and the precipitation associated with the cyclone (dark blue shading) (Dacre *et al.*, 2019). © American Meteorological Society. Used with permission.)

warm sector, where horizontal temperature gradients are weak (Dacre *et al.*, 2019). This cyclone airflow transports moist air horizontally towards the cyclone's cold front where moisture flux convergence leads to the formation of a filament of high total column water vapour (TCWV). Some of this moisture is transported towards the centre of the cyclone, where it supplies moisture to the base of the WCB. The remainder of the filament is transported away from the cyclone centre as it moves polewards.

Cyclone-relative airflows can also be described using Lagrangian trajectories. This technique involves following the path of parcels of air as they are transported in the atmosphere by the 3-dimensional wind fields. These trajectories can be clustered into airflows, such as the WCB, based on set criteria (Wernli and Davies, 1997; Wernli, 1997; Hart *et al.*, 2015). The analysis of winds on isentropic surfaces, or isentropic flow analysis, is an alternative technique analogous to Lagrangian trajectories. Both provide an indication of the structure of air streams within the cyclone (Browning and Roberts, 1994). However, isentropic flow analysis yields a snapshot of the field in time. Therefore, an estimate of pathways that are followed by air parcels for a short period of time (in the order of a few hours)

is provided. To compare results from studies that calculate trajectories to those performing isentropic flow analysis, both must be computed in the same frame of reference.

An alternative model for describing moisture transport in the extratropics was developed in the 1990s and is known as the atmospheric river model (Newell *et al.*, 1992). Atmospheric rivers are long, narrow and transient corridors of strong horizontal water vapour transport (Ralph *et al.*, 2018). They are identified by calculating the Eulerian vertically integrated moisture flux from the surface to the upper troposphere (known as vertically integrated vapour transport [IVT]). Typically, they are bounded by a fixed moisture flux threshold of $250\text{kgm}^{-1}\text{s}^{-1}$ although statistically defined thresholds have also been used (Shields *et al.*, 2018). Since they are defined using a vertically integrated measure, atmospheric rivers are 2-dimensional features. Atmospheric rivers have also been described using Lagrangian trajectories in an Earth-relative framework, for example in Pérez-Muñuzuri *et al.* (2018) and Sodemann *et al.* (2020).

The ascent necessary to convert water vapour within an atmospheric river into precipitation is typically invoked via the co-location of an atmospheric river with orography leading to forced ascent, or via co-location with cyclone WCBs leading to the moist isentropic ascent described above (as shown in the light blue shading in Figure 1). However, atmospheric rivers are identified in an Earth-relative framework, whereas the conveyor belt studies of Browning and Harrold (1970) and others are performed relative to moving cyclones. Therefore, it is difficult to directly relate atmospheric river flows to cyclone-relative WCB air streams and thus determine whether the identified moisture flux results in transport towards or away from the moving WCB at any given time. Despite these drawbacks, the atmospheric river model has proved to be a popular tool for examining the meridional transport of moisture from the subtropics to the extratropics (Gimeno *et al.*, 2014). The diagnostic to identify atmospheric rivers, IVT, does not require cyclone tracking and is calculated using widely available pressure level model output so is simpler to implement than cyclone-relative isentropic flow.

Significant statistical relationships have been found between atmospheric river strength and flooding events, which suggests that the atmospheric river model is a useful indicator of heavy precipitation. Dacre *et al.* (2019) investigated the relationship between IVT and cyclone precipitation in a climatology of 200 strong North Atlantic cyclones. They found that the moisture supplied to the base of the warm conveyor belt is not transported from where the atmospheric river feature met the reservoir of moist air in the subtropics (hereafter

termed non-local moisture), but instead was transported from the local environment through which the cyclone was travelling. Since cyclones typically travel with a velocity similar to the wind velocity at 700hPa (the steering level), they are moving faster than the moist boundary layer air through which they are travelling. As a result, the cold front sweeps up boundary layer moisture and the resulting moisture flux convergence creates a filament of high moisture content. The FA (green arrow in Figure 1) partitions this filament of moisture into a branch that accelerates towards the base of the warm conveyor belt and a branch that decelerates relative to the cyclone motion, and hence is 'left behind' by the poleward moving cyclone. High IVT is typically identified in both the accelerating and decelerating branches of the FA. Thus, moisture at the leading edge (within a few 100km) of an atmospheric river can provide moisture to the warm conveyor belt, but moisture along the main body of the atmospheric river, which can extend several thousands of kilometres, does not. Dacre *et al.* (2019) conclude that while high IVT is statistically related to cyclone precipitation, it is not correct to infer causation and interpret the correlation as atmospheric rivers transporting moisture from the subtropics to the centre of a cyclone. This conclusion is further supported by Papritz *et al.* (2021) who performed Lagrangian trajectory analysis in a cyclone-relative framework. Consistent with the cyclone-relative isentropic flow analysis of Dacre *et al.* (2019), they showed that moisture uptakes are linked to the cyclone's warm conveyor belt via the FA, a northeasterly cyclone-relative flow that arises due to the cyclone propagation exceeding the advection by the low-level background flow.

The study by Dacre *et al.* (2019) is based on composites of 200 cyclones. Cyclone compositing is a powerful method, which emphasises features that are common to the cyclones while de-emphasising features that are not. However, it is possible that the composite fields do not represent the airflows in the individual cyclones that contribute to the composite. Therefore, the aim of this article is to objectively identify the FA in a case study of storm *Bronagh*. To do so, we develop an identification diagnostic that detects the saddle point¹ created by the FA and DI using cyclone-relative isentropic flow. This analysis is performed at each stage in storm *Bronagh's* evolution to ascertain where moisture is transported from at different stages in the storms development.

¹A point at which a function of two variables has partial derivatives equal to zero but at which the function has neither a maximum nor a minimum value (Collins English Dictionary, 2005).

Dataset and cyclone tracking algorithm

This study uses the ERA5 atmospheric reanalysis dataset (Hersbach *et al.*, 2020), which has a spatial resolution of approximately 31km. At the surface and on isobaric surfaces, the data are interpolated onto a longitude–latitude grid with 0.25° resolution, and on isentropic surfaces, the data are interpolated on a grid with 1° spatial resolution. This resolution is sufficient given that this study is focused on large-scale circulation. Three-hourly temporal resolution is used to determine the moisture flux on pressure and isentropic surfaces.

Several single-level reanalysis fields are also analysed. TCWV (kgm^{-2}) is the total amount of water vapour in a column extending from the surface of the Earth to the top of the atmosphere. The vertical integral of eastward and northward water vapour fluxes ($\text{kgm}^{-1}\text{s}^{-1}$) represents the horizontal rate of flow of water vapour, in the eastward/northward direction, per metre across the flow, for a column of air extending from the surface of the Earth to the top of the atmosphere. Positive values indicate a flux from west to east or south to north, respectively. The vertical integral of eastward and northward vapour fluxes are the vector components of vertically integrated moisture flux (IVT), which is used to identify atmospheric rivers using a threshold of $250\text{kgm}^{-1}\text{s}^{-1}$ (see e.g. Shields *et al.*, 2018, and references therein).

The track position of storm *Bronagh* in the ERA5 dataset is identified using the tracking algorithm of Hodges (1995). The track of storm *Bronagh* is identified using three-hourly 850hPa-relative vorticity, truncated to T42 resolution to emphasise the synoptic scales. The 850hPa relative vorticity features are filtered to remove stationary or short-lived features that are not associated with extratropical cyclones. The track is used to find the minimum pressure at every time-step by searching for the minimum mean sea-level pressure in a 500km radius around the relative vorticity maximum. The track positions at three-hourly intervals are also used to compute the cyclone's propagation velocity using a centred finite difference approximation.

Storm *Bronagh*

Storm *Bronagh* was an extratropical cyclone that originated south of Newfoundland on 19 September 2018. It tracked eastwards across the North Atlantic (red track in Figure 2b) deepening from 1008 to 986hPa (Figure 2a) as it passed over the UK on 21 September 2018. During this time, storm *Bronagh* caused localised flooding in parts of England and Wales where daily rainfall totals exceeding 50mm were recorded in

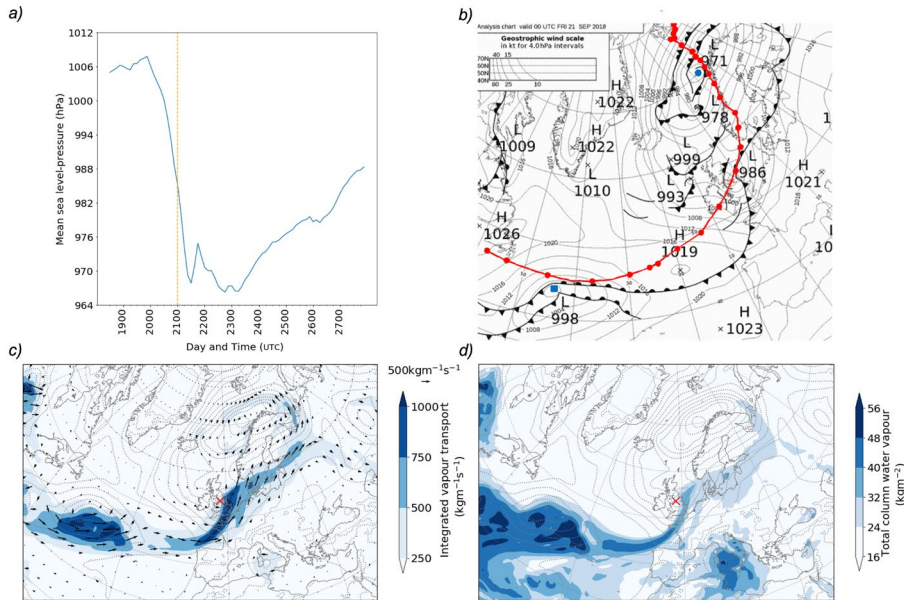


Figure 2. (a) Evolution of storm Bronagh's central mean sea-level pressure (hPa). The vertical line corresponds to 0000 UTC 21 September 2018. (b) Met Office surface analysis chart at 0000 UTC on 21 September 2018 (© 2018 Crown copyright). The red solid line represents storm Bronagh's track. Red circles show the position of the cyclone's centre at six-hourly intervals. The blue circle represents the centre of storm Ali, the red cross represents storm Bronagh's centre and the blue square represents the cyclone centre of storm C at 0000 UTC on 21 September 2018. (c) ERA5 IVT (filled contours and vectors) and (d) ERA5 TCWV (filled contours) at 0000 UTC on 21 September 2018. Panels (c) and (d) are overlaid with ERA5 mean sea-level pressure (grey contours).

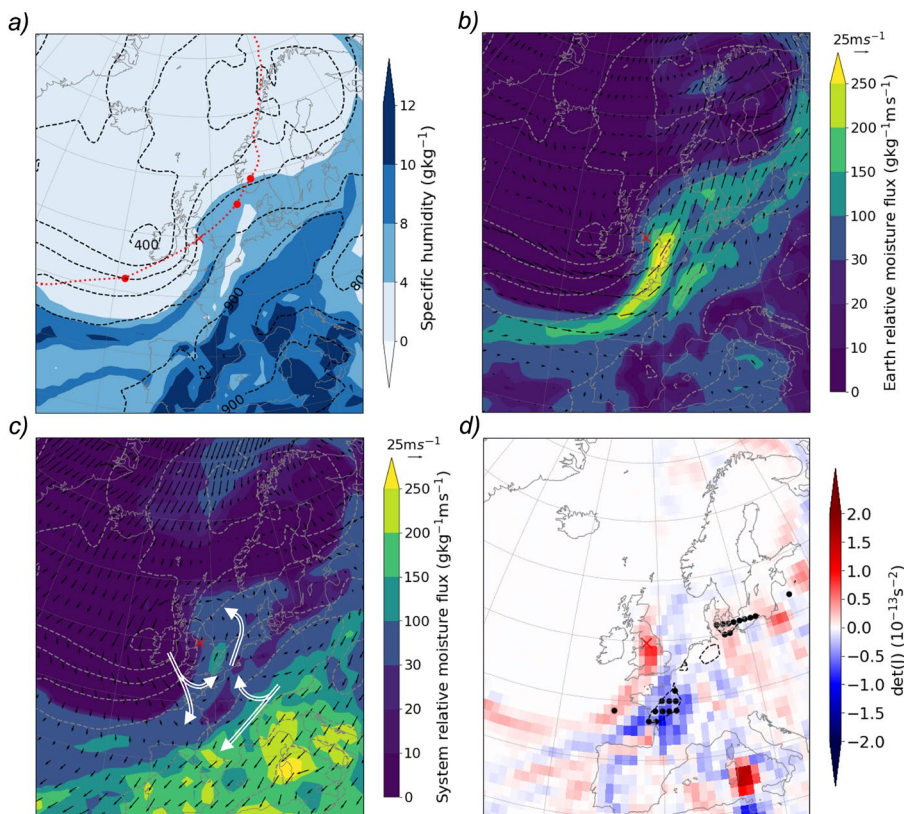


Figure 3. Fields on the 300K isentropic surface. (a) Pressure (hPa, dashed contours) and specific humidity (filled contours) overlaid with storm Bronagh's track (red dashed). The cyclone centre at 0000 UTC 21 September 2018 is marked by a red cross. The centre of the storm at 1200 UTC 20 September 2018, 0900 UTC 21 September 2018 and 1500 UTC 21 September 2018 (red dots) are shown from left to right, respectively. (b) Earth-relative moisture flux (shaded), pressure (hPa, dashed contours) and Earth-relative horizontal wind (arrows). (c) Cyclone-relative moisture flux (shaded), pressure (hPa, dashed contours) and cyclone-relative horizontal wind (black arrows) overlaid with position of cyclone airflows (white arrows). (d) $\det(\mathbf{J})$ (shaded) and the 5th percentile in cyclone-relative moisture flux (dashed line). This panel also includes the minima identified by the watershed algorithm (black dots).

upland areas of Wales, the southern Pennines and North York Moors (Met Office, 2018). The extreme rainfall and winds associated with storm *Bronagh* led to travel disruptions throughout the UK. Following this, storm *Bronagh* continued to track northeastwards and deepen further. Its minimum mean sea-level pressure of 968 hPa occurred at 1800 UTC on 22 September 2018 over the Norwegian Sea (Figure 2a).

Storm *Bronagh* occurred during a period of intense cyclonic activity in the North Atlantic, starting with post-tropical cyclone *Helene*, which passed over the UK on 17 September 2018 (Gentile *et al.*, 2021). This was followed by storm *Ali* on 18 September and then storm *Bronagh* on 20/21 September. The decaying storm *Ali* can be seen to the north of storm *Bronagh* in Figure 2(b) with a central pressure of 971 hPa. A third cyclone in its developing stage with a central pressure of 998 hPa can also be seen in Figure 2(b) in the mid-North Atlantic (43°W, 44°N) (hereafter storm C). Storm *Ali*, storm *Bronagh* and storm C form a family of extratropical cyclones with each subsequent cyclone forming on the trailing cold front of the previous cyclone. Associated with storm *Ali*, storm *Bronagh* and storm C is a filament of IVT exceeding $250 \text{ kg m}^{-1} \text{ s}^{-1}$ (Figure 2c) and a corresponding filament of enhanced TCWV (Figure 2d). Thus, an atmospheric river of several thousands of kilometre length and a few 100 km width can be identified originating at 30°N and extending across the North Atlantic and into northwest Europe (ending around 70°N). The moisture flux within the atmospheric river is higher in the vicinity of storm *Ali*, storm *Bronagh* and storm C due to the increased horizontal pressure gradients and hence increased wind speeds associated with each cyclone. Similar analysis has been performed at earlier and later times and at all stages in storm *Bronagh*'s lifecycle an atmospheric river is identified in the vicinity of the storm (not shown).

As described in the introduction, IVT alone cannot be used to determine if moisture originating at the start of the atmospheric river is transported into the centre of storm *Bronagh* to produce the heavy precipitation associated with the storm. To determine where moisture leading to precipitation is transported from, it is necessary to calculate the moisture flux in the frame of reference of the moving cyclone. In the following section, we calculate the cyclone-relative flow and moisture flux on the 300K isentropic surface.

Cyclone-relative isentropic flow

Figures 3(a–d) show fields in a domain that is centred on the position of storm *Bronagh* at 0000 UTC on 21 September 2018 (red cross in Figure 3a). Figure 3(a) shows pressure on the 300K isentropic surface. The 300K isentropic surface slopes in the vertical from

below 800hPa in the cyclone's warm sector to 300hPa in the cold sector. The steepest slopes are co-located with the position of the cyclone's cold and warm fronts. Figure 3(a) also shows the specific humidity on the 300K surface within the domain. As expected, relatively high specific humidity values are found closer to the surface, below 700hPa.

Moisture flux (wind vectors multiplied by specific humidity) and wind vectors on the 300K isentropic surface in an Earth-relative framework are shown in Figure 3(b). Moisture flux on this isentropic surface is highest to the south of the cyclone centre in a band extending along the cyclone's cold front. This is similar to the IVT shown in Figure 2(c). Assuming a stationary cyclone, in an Earth-relative framework the flow on the 300K isentropic surface appears to descend behind the surface cold front, cross the cold front boundary and then to ascend over the surface warm front. However, the storm is not stationary but is travelling towards the northeast at about 19ms^{-1} . Therefore, the cyclone velocity is of a similar magnitude and direction to the wind vectors within the region of high earth-relative moisture flux.

Moisture flux and wind vectors on the 300K isentropic surface in a cyclone-relative framework are shown in Figure 3(c). The cyclone-relative moisture flux and wind vectors are calculated by subtracting the cyclone velocity from the wind vectors. In the cyclone-relative framework, the flow on the isentropic surface looks very different. To the west of the cyclone centre, air descends from 400 to 700hPa along the sloping isentropic surface. At this point, the airflow splits into two branches. One branch turns cyclonically towards the cyclone centre at 700hPa. The other branch descends further to 800hPa and turns anticyclonically away from the cyclone centre. This dry cyclone-relative airflow is the DI shown in Figure 1. To the east of the cyclone centre, air ascends from 800 to 500hPa where it then turns cyclonically and wraps around the cyclone centre. This moist cyclone-relative airflow is the WCB shown in Figure 1. To the southeast of the cyclone centre, the cyclone-relative airflow on the 300K isentropic surface is confined to the lower troposphere, 850–950hPa. This airflow is directed towards the cold front where it splits into two branches. One branch turns towards the cyclone centre and ascends slightly. The other branch travels parallel to the surface cold front directed away from the cyclone centre. This moist low-level airflow is the FA shown in Figure 1.

At the interface between the DI and the FA, there is a saddle point in the cyclone-relative flow and therefore, there is a region where the flow becomes stationary. As a result, the isentropic cyclone-relative moisture flux is small in this region. In Figure 3(c), cyclone-relative moisture fluxes

smaller than $30\text{gkg}^{-1}\text{ms}^{-1}$ are observed over northwest France indicating the position of the saddle point. The presence of a saddle point within the identified atmospheric river (as shown in Figure 2c) shows that only moisture within the portion of the atmospheric river downstream of the saddle point (i.e. between the saddle point and the cyclone centre) can be transported into the centre of the cyclone. Moisture within the portion of the atmospheric river upstream of the saddle point is not travelling as fast as the cyclone itself so will get further from the cyclone as it travels, effectively being left behind by the poleward moving cyclone.

Saddle point identification diagnostic

In this section, an algorithm for objectively identifying saddle points in lower-tropospheric cyclone-relative airflows that occur in the warm sector of storm *Bronagh* is described. The algorithm is developed so that it can automatically be applied to many

cyclones in future work. In order to focus on lower-tropospheric airflows, the search is confined to the portion of the isentropic surface that is below 800hPa within 2000km of the cyclone centre. Within this part of the surface, regions where the cyclone-relative moisture flux is small, that is within the lowest 5% of values are identified using a watershed algorithm (Najman and Schmitt, 1994) (see Box 1). To differentiate the minima found by the watershed algorithm in the cyclone-relative moisture flux that are associated with low specific humidity from those that are associated with saddle points, locations where the Jacobian determinant of the moisture flux field, $\det(\mathbf{J})$, is negative (see Box 2) are identified. This latter criterion comes from non-linear systems theory for the classification of hyperbolic fixed points (e.g. figure 6.4 in Drazin, 1992).

The criteria above applied to storm *Bronagh* at 0000 UTC on 21 September 2018 are shown in Figure 3(d). The contour corresponding to the lowest 5% of cyclone-relative moisture flux values on the 300K isentropic surface

Box 1. The detection of minima in the moisture flux field

To evaluate the Jacobian determinant of the linearised moisture flux at a fixed point, the fixed points must firstly be identified in an objective manner. To do so, an image segmentation tool called the watershed algorithm is used. This algorithm treats the field of interest like topography such that the minima of interest are depicted as basins. To find different basins, the topography is submerged in a lake so that each basin fills up with water according to their depth. The location in which the water meets marks the edge of each basin. Therefore, the location and area that the minima span is known. To define how much the topography is submerged, and therefore, the area that the identified minima span, a threshold value is used (Najman and Schmitt, 1994).

Box 2. The detection of saddle points and the FA

To develop an identification algorithm for the presence of saddle points associated to a FA at a given time during the evolution of the cyclone, the instantaneous configuration of the cyclone-relative low-level moisture flux is relied upon. If present, the FA splits into two branches on approach to the system's cold front (Figure 1). A branch with a southerly component will then feed moisture into the system's WCB. A branch with a northerly component will tend to leave the cyclone's immediate neighbourhood and transport moisture rearwards with respect to the cyclone centre. The moisture flux vector field near the splitting point will constitute a fixed point, that is, a point for which the vector field is zero, and will have a similar configuration to that of a saddle point in the phase space of linearised second-order differential systems (e.g. figure 6.4 in Drazin, 1992). Therefore, the Jacobian determinant of the isentropic moisture flux is calculated using the classification of fixed points from non-linear systems theory (see e.g. Drazin, 1992). This determinant is given by

$$\det(\mathbf{J}) = \frac{\partial(qu)}{\partial x} \frac{\partial(qv)}{\partial y} - \frac{\partial(qu)}{\partial y} \frac{\partial(qv)}{\partial x}, \quad (1)$$

where u and v are the eastward and northward components of wind, respectively, x and y are the eastward and northward pointing coordinates, respectively, and q is the specific humidity, all on an isentropic surface. According to this method, a saddle point will be characterised by a negative Jacobian determinant of the linearised moisture flux when evaluated at a fixed point. The partial derivatives in the Jacobian determinant on the longitude–latitude grid are calculated using a centred difference approach such that the determinant is calculated over a grid with 200km grid spacing.

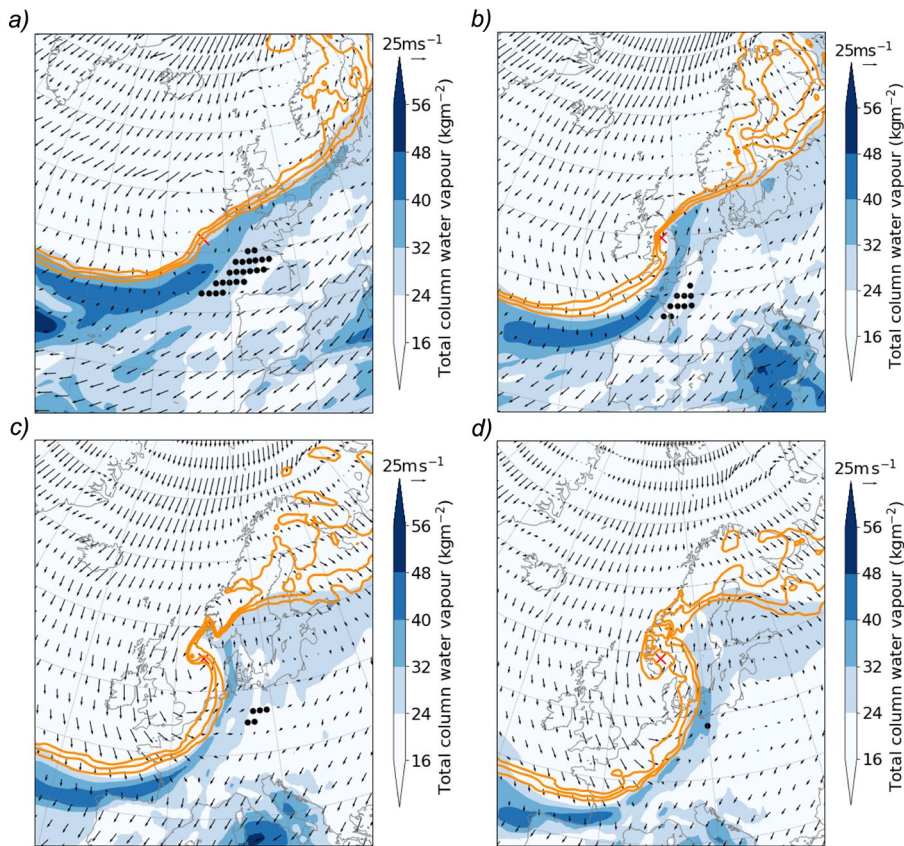


Figure 4. TCWV (filled contours), saddle points (black dots) and cyclone-relative wind vectors on the 300K isentropic surface at (a) 1200 UTC 20 September 2018, (b) 0000 UTC 21 September 2018, (c) 0900 UTC 21 September 2018 and (d) 1500 UTC 21 September 2018. The panels also include the 290, 292 and 294K potential temperature contours at 850hPa (orange contours).

(below 800hPa) is represented by the dashed contours. Low cyclone-relative moisture flux values are found behind the cold front and ahead of the warm front where specific humidity decreases due to the sloping nature of the isentropic surfaces. Low cyclone-relative moisture flux values are also found in a small region ahead of the cold front. Identified cyclone-relative moisture flux minima are shown in black dots. Finally, $\det(\mathbf{J})$ is calculated and negative values co-located with the minima are searched for, indicating saddle points in the moisture flux field. Only the moisture flux minima to the south of the cyclone centre satisfy all of the criteria so are identified as saddle points. This region is indeed co-located with the region identified in Figure 3(c) at the interface between the FA and the DI.

The feeder air stream in storm Bronagh

Figure 4 shows the location of identified saddle points in the 300K isentropic cyclone-relative moisture flux at various times in the evolution of storm Bronagh. The fields are centred on the cyclone positions as shown in Figure 3(a). At all stages, the regions identified as saddle points are located in the cyclone's warm sector ahead of the cold front. In Figure 4(a), the region

associated with the saddle point is situated south of the cyclone centre. However, as the storm evolves, the saddle point moves eastwards and the cold front becomes more meridionally oriented as shown in Figures 4(b–d). Furthermore, these saddle points are found at the leading edge of the filament of high TCWV. The cyclone-relative moisture flux in the part of the filament upstream of the saddle point is directed away from the cyclone centre indicating that moisture in this part of the filament is travelling slower than the cyclone. Thus, this moisture cannot feed into the base of the ascending WCB and therefore, will remain in the lower atmosphere. Conversely, the cyclone-relative moisture flux downstream of the identified saddle points is directed towards the cyclone centre and will feed into the WCB where it will ascend leading to the formation of clouds and precipitation. This is supported by the decrease in TCWV around the saddle point with time. In Figure 4(a), there is greater than 40kgm^{-2} within the vicinity of the FA, however by Figure 4(d), this has decreased.

Conclusions

In this paper, an algorithm for identifying the FA in a case study of storm Bronagh is described and the results for the identification

of the FA throughout the evolution of the storm are presented. Storm Bronagh was responsible for flooding and strong winds in the UK on 20/21 September 2018. Using a threshold of vertically integrated moisture flux, an atmospheric river associated with this storm is identified and the characteristic cyclone airflows (DI, WCB and FA) are also identified using isentropic cyclone-relative flow. In order to ascertain where the moisture responsible for storm Bronagh's precipitation is transported from, a diagnostic is developed to identify the presence of saddle points in the cyclone-relative moisture flux field. These saddle points occur at the interface of the descending DI behind the cold front and the low-level FA ahead of the cold front. The presence of a saddle point within the identified atmospheric river indicates that moisture upstream of the saddle point cannot contribute to the moisture ascending in the WCB. Absence of a saddle point within an atmospheric river indicates that moisture within the atmospheric river can be transported to the base of the WCB and thus contributes to large-scale precipitation.

Applying the saddle point diagnostic to the evolution of storm Bronagh shows that saddle points are identified within the atmospheric river during its passage over the UK and northwest Europe. The presence of such saddle points indicates that moisture is transported to the WCB in storm Bronagh from in the local environment in which Bronagh is developing and not from the start of the atmospheric river in the subtropics. Future work will include applying this diagnostic to a large set of cyclones to construct a climatology of the FA. This large set will include cyclones with varying intensity, genesis location and cyclone types to determine systematically when and where a FA is present.

The diagnostic developed in this paper only determines where the moisture contributing to large-scale precipitation is transported from. It is plausible that forced ascent of moist air in the atmospheric river over the hills in the UK may also have led to the formation of orographically generated precipitation. Future work will include simulations of study of storm Bronagh using the UK Met Office 1.5km resolution numerical weather prediction model to determine the relative contributions of large-scale precipitation associated with the WCB ascent and locally forced precipitation associated with orographic ascent.

References

- Allan RP, Soden BJ. 2008. Atmospheric warming and the amplification of precipitation extremes. *Science* **321**: 1481–1484.
- Browning K. 1971. Radar measurements of air motion near fronts. *Weather* **26**: 320–340.
- Browning K, Harrold T. 1970. Air motion and precipitation growth at a cold front. *Q. J. R. Meteorol. Soc.* **96**: 369–389.

Browning KA, Roberts NM. 1994. Structure of a frontal cyclone. *Q. J. R. Meteorol. Soc.* **120**: 1535–1557.

Carlson TN. 1980. Airflow through midlatitude cyclones and the comma cloud pattern. *Mon. Weather Rev.* **108**: 1498–1509.

Collins English Dictionary. 2005. Definition of saddle point [accessed 14 March 2022. Most material © 2005, 1997, 1991 by Penguin Random House LLC. Modified entries © 2019 by Penguin Random House LLC and HarperCollins Publishers Ltd. Word origin [1920–25]].

Dacre HF, Clark PA, Martínez-Alvarado O et al. 2015. How do atmospheric rivers form? *Bull. Am. Meteorol. Soc.* **96**: 1243–1255.

Dacre HF, Martínez-Alvarado O, Mbengue CO. 2019. Linking atmospheric rivers and warm conveyor belt airflows. *J. Hydrometeorol.* **20**: 1183–1196.

Drazin PG. 1992. Nonlinear systems. In: *Cambridge Texts in Applied Mathematics*. Cambridge University Press: Cambridge, UK.

Gentile ES, Gray SL, Barlow JF et al. 2021. The impact of atmosphere–ocean–wave coupling on the near-surface wind speed in forecasts of extratropical cyclones. *Bound. Layer Meteorol.* **180**: 105–129.

Gimeno L, Nieto R, Vázquez M et al. 2014. Atmospheric rivers: a mini-review. *Front. Earth Sci.* **2**: 2.

Hart NC, Gray SL, Clark PA. 2015. Detection of coherent airstreams using cluster analysis: application to an extratropical cyclone. *Mon. Weather Rev.* **143**: 3518–3531.

Hersbach H, Bell B, Berrisford P et al. 2020. The ERA5 global reanalysis. *Q. J. R. Meteorol. Soc.* **146**: 1999–2049.

Hodges KI. 1995. Feature tracking on the unit sphere. *Mon. Weather Rev.* **123**: 3458–3465.

Lavers DA, Allan RP, Wood EF et al. 2011. Winter floods in Britain are connected to atmospheric rivers. *Geophys. Res. Lett.* **38**: 1–8.

Lavers DA, Villarini G, Allan RP et al. 2012. The detection of atmospheric rivers in atmospheric reanalyses and their links to British winter floods and the large-scale climatic circulation. *J. Geophys. Res. Atmos.* **117**: D20106. <https://doi.org/10.1029/2012JD018027>

Met Office. 2018. Strong winds and heavy rain from storms ali and bronagh. <https://www.metoffice.gov.uk/binaries/content/assets/metofficegovuk/pdf/weather/learn-about/uk-past-events/interesting/2018/strong-winds-and-heavy-rain-from-storms-ali-and-bronagh---met-office.pdf> [accessed 25 November 2021].

Najman L, Schmitt M. 1994. Watershed of a continuous function. *Signal Process.* **38**: 99–112.

Newell RE, Newell NE, Zhu Y et al. 1992. Tropospheric rivers? A pilot study. *Geophys. Res. Lett.* **19**: 2401–2404.

Papritz L, Aemisegger F, Wernli H. 2021. Sources and transport pathways of precipitating waters in cold-season deep north Atlantic cyclones. *J. Atmos. Sci.* **78**: 3349–3368.

Pérez-Muñuzuri V, Eiras-Barca J, Garaboa-Paz D. 2018. Tagging moisture sources with Lagrangian and inertial tracers: application to intense atmospheric river events. *Earth Syst. Dyn.* **9**: 785–795.

Pfahl S, Wernli H. 2012. Quantifying the relevance of cyclones for precipitation extremes. *J. Clim.* **25**: 6770–6780.

Ralph FM, Dettinger MD, Cairns MM et al. 2018. Defining “atmospheric river”: how the Glossary of Meteorology helped

resolve a debate. *Bull. Am. Meteorol. Soc.* **99**: 837–839.

Shields CA, Rutz JJ, Leung L-Y et al. 2018. Atmospheric river tracking method intercomparison project (ARTMIP): project goals and experimental design. *Geosci. Model Dev.* **11**: 2455–2474.

Sodemann H, Wernli H, Knippertz P et al. 2020. *Structure, Process, and Mechanism*. Springer: New York, NY, pp 15–43.

Wernli H. 1997. A Lagrangian-based analysis of extratropical cyclones. II: a detailed case-study. *Q. J. R. Meteorol. Soc.* **123**: 1677–1706.

Wernli H, Davies H. 1997. A Lagrangian-based analysis of extratropical cyclones. I: the method and some applications. *Q. J. R. Meteorol. Soc.* **123**: 467–489.

Young MV, Monk GA, Browning KA. 1987. Interpretation of satellite imagery of a rapidly deepening cyclone. *Q. J. R. Meteorol. Soc.* **113**: 1089–1115.

Correspondence to: S. Cuckow


s.cuckow@pgr.reading.ac.uk

© 2022 The Authors. *Weather* published by John Wiley & Sons Ltd on behalf of the Royal Meteorological Society

This is an open access article under the terms of the Creative Commons Attribution License, which permits use, distribution and reproduction in any medium, provided the original work is properly cited.

doi: 10.1002/wea.4212

North Atlantic Oscillation response to the Madden–Julian Oscillation in a coupled climate model

Daniel T. Skinner¹ ,
Adrian J. Matthews^{1,2} ,
and David P. Stevens¹ 

¹Centre for Ocean and Atmospheric Sciences, School of Mathematics, University of East Anglia, Norwich, UK

²Centre for Ocean and Atmospheric Sciences, School of Environmental Sciences, University of East Anglia, Norwich, UK

Introduction

The Madden–Julian Oscillation (MJO; Madden and Julian, 1971) is the leading

mode of intra-seasonal variability in the tropics and is characterised by an area of enhanced deep convection, which travels eastward across the Maritime Continent with a period of 30–60 days. This area of enhanced convection is associated with divergence in the upper troposphere and is followed directly by an area of suppressed convection associated with convergence in the upper troposphere.

This divergent circulation produced by latent heat release in the MJO's enhanced convective phase excites Rossby waves, which interact with various extratropical weather regimes to create so-called teleconnection patterns. Through these teleconnections, the weather experienced around

the globe can be linked back to the weather in the tropics.

The North Atlantic Oscillation (NAO; Walker and Bliss, 1932) is a key mode of winter variability in northern Europe. Thus, understanding the behaviour of the NAO is key to accurate United Kingdom (UK) weather prediction. The NAO is characterised by a positive and a negative phase, which bring different types of weather to the UK. During the winter, the NAO+ is associated with warmer, stormier weather, while the reverse relationship is observed for the NAO–.

Through observational studies, the NAO is known to be forced at least in part by the MJO (Cassou, 2008; Lin *et al.*, 2010). In this